Pakistan Journal of Medical & Cardiological Review
https://pakjmcr.com/index.php/1/about
Online ISSN 3007-2387
Print ISSN 3007-2379

Synthesis and Characterization of Zinc-Doped Carbon Dots for Enhanced Fluorescence Applications

Sabahat Asghar (Corresponding Author)
Khwaja Fareed University of Engineering and Information Technology, Rahim Yar Khan, Pakistan Email: sabahatasgharofficial@gmail.com

Dr. Muhammad Arsalan Dilbraiz
Department of Applied Sciences, Pakistan Navy Engineering College (PNEC), National University of Science and Technology (NUST), Karachi Campus, Pakistan Email: arsalan.dilbraiz@pnec.nust.edu.pk

Syed Qasim Mehmood
Department of Pharmacy, Comsats University Islamabad, Abbottabad Campus, Pakistan Email: syedqasimshah99@gmail.com

Author Details

Corresponding E-mail & Author*:

Sabahat Asghar
Khwaja Fareed University of Engineering and Information Technology, Rahim Yar Khan, Pakistan Email: sabahatasgharofficial@gmail.com

Keywords: Zinc-Doped Carbon Dots (Zn-CDs), Fluorescence Improvement, Quantum Yield, Band Gap Narrowing, Surface Passivation, Photoluminescence, Hydrothermal Synthesis, Photostability, Bioimaging Applications, Optoelectronic Nanomaterials.

Received on 10 Dec 2025
Accepted on 10 Jan 2026
Published on 22 Jan 2026

Abstract

In the current study, we prepared zinc-doped carbon dots (Zn-CDs) through a one-step hydrothermal method using citric acid and urea as precursors, and carbon and urea as the sources of dopant, respectively. TEM images showed that the resultant nanoparticles had a mean diameter of 3.6 ± 0.5 nm. Ultraviolet in visible spectroscopy showed that there was a strong absorption band at 360nm, which showed the presence of pi-pi transitions. The photoluminescence emission had a peak of 445 nm, which was attained at excitation of 365 nm. The Zn-CDs exhibited 52.8 per cent enhancement of the fluorescence intensity as well as a quantum yield of 38 percent, which is nearly 1.6 times greater than that of undoped carbon dots. The incorporation of Zn^{2+} ions was confirmed by Fourier-transform infrared (FTIR) spectroscopy, with binding-energy peaks centred at approximately 1022.1 eV (Zn 2p 3/2) and 1045.2 eV (Zn 2p 1/2). The effect of improved surface passivation and zinc-induced defect states that will provide a radiative recombination mechanism can explain the observed enhancement of photoluminescence. It was also found that the synthesized Zn2-CDs were highly photostable, with over 95 per cent of their fluorescence remaining intact following 120 min of continuous UV irradiation, illustrating their future use in optical sensing and bioimaging.

Introduction

Carbon-based quantum dots (CDs) form an increasingly popular category of fluorescent nanomaterials, typically smaller than 10nm. They have unique optical and electrical properties such as size-dependent emission, chemical stability, and

biocompatibility. Since their original publication in 2004, CDs have received significant attention as alternatives to standard semiconductor quantum dots as a relatively inexpensive substitute, the dots of which frequently include toxic heavy metals such as cadmium or lead. However, the pristine CDs usually exhibit low quantum yields (QY) that are less than 150 rates, weakened photoluminescence, and low emission stability, thus limiting their usage in biomedicine, sensing, and light-emitting technologies. Another method that has been suggested to overcome such drawbacks is heteroatom doping to tune the electronic structure and surface chemistry of CDs. The formation of dopant species provides the impurity levels of energy that affect the recombination process of the photogenerated charge carriers, which leads to an increase in the radiative transitions. Some of the metal ions investigated have included Zn^{2+}, Cu^{2+}, Mn^{2+}, and Fe^{2+}, which have shown to be especially useful in increasing fluorescence efficiency. Wang et al. (2023) claimed that Zn doping enhanced the intensity of the emission of CDs by 52%, and Kumar et al. (2025) found that Zn incorporation increased the quantum yield by 19 to 36%. Li et al. (2024) have shown that ZnC interactions increase the fluorescent lifetime by about 1.8ns, and thus proved the presence of zinc passivation of surface trap states. The $3d^{10}$ electronic configuration of the Zn^{2+} ion allows it to react well with the carbon core without creating deep trap states to kill luminescence. Additionally, Zn^{2+} is a benign, environmentally and biologically compatible dopant, which is useful in biosensing and fluorescence-based diagnostics. Chen et al. (2025) also demonstrated that Zn-loaded CDs do not lose more than 90 percent of their fluorescence strength after 2 hours of uninterrupted UV radiation exposure, which further demonstrates that it is more photostable than both nitrogen and sulfur doped analogues.

A combination of several processes plays a role in the observed enhancement of fluorescence with Zn doping: (i) surface passivation, reducing non-radiative recombination centers; (ii) energy-level alignment, whereby Zn-induced defect states act as shallow traps, which enhance radiative recombination; and (iii) a minor change in the electronic structure, which decreases the band gap, thereby increasing the likelihood of electron-hole recombination. The experimental evidence also shows that the concentration of the precursor of Zn can be used to tune the emission peak to either 420 nm or 490, allowing multi-color emission to be used in optoelectronics. Zn -doping protocols are proven and effective as reported quantum -yield improvements of 40 -65% in publications as of 2023 and 2025. However, the mechanism and extent of incorporation of zinc that affect the structural and optical characteristics of the CDs by various synthetic pathways are still unclear. The differences observed in reports are usually explained by the differences in the ratios of the precursors, temperature of the reaction, or the source of carbon used. This paper, therefore, seeks to prepare Zn-dotted carbon dots through a controlled hydrothermal method at 180 ^{0}C temperature with an elaborate characterization package including TEM, FTIR, XPS, UV-Vis, and fluorescence spectroscopy. We will examine the influence of Zn inclusion on emission intensity, quantum yield, and photostability systematically with the view of unraveling the underlying photophysical processes involved in causing fluorescence to increase.

Materials and Methods

Materials

We used all of the reagents in their purest analytical form without additional purification. It was synthesised using the following materials: citric acid ($C_6H_8O_7$) as a carbon precursor (≥ 99.5% Sigma-Aldrich); urea (CH_4N_2O) as a nitrogen source and mild reducing agent (≥ 99.5% Merck); zinc nitrate hexahydrate (Zn (NO_3) $2H_2O$) as the Zn dopant (≥ 98% Sigma-Aldrich); and deionised water

Zinc-Doped Carbon Dots
Synthesis of zinc-Darabontate (Zn0.05) or Zinc- Tetrazole (Zn0.5) of Carbon Dots is prepared by incubating the biosensor with 20 ml of 0.1 M Zinc Chloride.
The hydrothermal route was selected due to its simplicity, reproducibility, and ability to produce nanoparticles of similar size.

The precursor solution should be prepared.
Citric acid and urea were dissolved in 30mL of deionised water to give a solution, where 2.00g of citric acid and 1.00g of urea were used. A molar ratio of C: Zn of about 25:1 of zinc nitrate hexahydrate (Zn $(NO_3)_2$ $6H_2O$ (0.10g of Zn) was timely added to attain the desired loading of Zn. A slight portion of NaOH was added to the solution to adjust the pH to 6.8–0.2 and achieve the homogeneous distribution of the Zn^{2+} ions.

Hydrothermal treatment
A 50-mL stainless-steel Teflon-coated autoclave was used to transfer the homogeneous precursor solution to it. The autoclave was closed and put in a muffle furnace at 180 °C for 6 h. On completion, the system was left to cool to ambient temperature to yield a dark-brown colloidal suspension.

Purification
The colloid was initially filtered using a 0.22 -membrane to eliminate large particles. After that, the filtrate was dialysed (cut-off of 1-kDa) with deionised water over 24 h to remove precursors and by-products that were not reacted.
We freeze-dried the purified Zn-CD solution to produce a dry powder for further testing.

Control Sample
We prepared undoped carbon dots (CDs) in the same conditions, but with the exception of Zn ($NO_{32}OH_2O$), in order to arrive at a clear comparison basis.

Determination of Reaction Yield
The reaction yield was determined through the use of the mass-energy balance method.
The relationship used to compute the synthesis yield was as follows:

$$Y(\%) = \frac{m_p}{m_r} \times 100$$

Where: = mass of purified Zn-CDs acquired (g)
 = the aggregate mass of the carbon precursor used (g)
The outcome was measured between 32, 0 -38, 0 -34, depending on the Zn^{2+} concentration in the reaction medium.

Measurement of Quantum Yield (QY)
Quinine sulphate (0.54 in 0.1 M H 2 SO 4) was used as the reference standard to measure the quantum yield (0.54) of Zn -CDs.
Where: Φ_s = Quantum Yield of Zn-Cadmium Sulphide
 Φ r QY of conventional quinine sulphate
I_s and I_r = the aggregate fluorescence intensity of the sample and the reference
As, Ar = absorbance values at the excitation wavelength (≤0.1 to minimise reabsorption)
, , = the refractive indices of solvents (e.g., water = 1.33 and H_2SO_4 = 1.33)

The quantum yield of the Zn-CDs was 38-2% (2.32 times higher than in the case of undoped CDs), which was 23-2%.

Characterization Techniques

Transmission Electron Microscopy (TEM)

The morphology and the size of the particles of the ZnCDs were analyzed using a JEOL JEM-2100 that was run at 200kV. The drop-casting of a 0.1mg/mL aqueous dispersion on carbon-coated copper grids with the subsequent vacuum drying was used to prepare the samples. A diameter of 3.6.5nm was obtained after analysis of 200 particles.

UV–Vis Spectroscopy

The optical absorption spectra were collected at a Shimadzu UV 2600 spectrometer at wavelengths between 200 and 800nm. Zn 2 CDs had a strong absorption at 360 29nm, which was assigned to pp^{+} transitions in sp^{2} high domains, and a shoulder at 280 29nm, the npp^{+} transitions of the C=O moieties on surfaces.

Photoluminescence (PL) Spectroscopy

FTIR spectra ($4000400cm^{-1}$) were obtained with a PerkinElmer Spectrum -100 and KBr pellets. The presence of carboxyl and hydroxyl functionalities was ascertained through the presence of the 1730 cm^{-1} (C=O), 1220 cm^{-1} (C-O), and 3420 cm^{-1} (O-H) peaks. The appearance of a new band at 420 cm^{-1} suggested the formation of a Zn-O bond, which was a successful doping.

X-ray Photoelectron Spectroscopy (XPS)

Incidence of Zn 2p 3/2 and Zn 2p 1/2 at 1022.1 and 1045.2 eV, respectively, indicated the incorporation of $2p + Zn^{2}$ in Thermo Scientific ESCALAB 250Xi with Al K (1486.6 eV) radiation. C 1s, O 1s, and N 1s spectra revealed that there were bonding motives that were consistent with a carbon-oxygen-nitrogen structure.

Photostability and Fluorescence Retention Tests

Zn-CDs $0.5mg/ml^{-1}$ were irradiated with UV565nm (10W) light, and after 120min, the sample fluorescence decreased by 5 per cent compared to undoped CDs, which decreased by 3 per cent. This shows the excellent optical stability of the doped material.

Results and Discussion

Morphology and Structural Characteristics

TEM images show Zn-doped CDs to be almost spherical, homogeneous, and the mean size is 3.6 0.5nm. Lattice fringes are viewed at high resolution in images with a spacing of 0.21^{-1}nm, which is equal to the (100) plane of a graphitic carbon structure. This small diameter increase (3.4 ± 0.6 nm compared to undoped CDs) can be explained by Zn^{2+}-induced adjustment of nucleation kinetics by hydrothermal synthesis. None of the aggregation or formation of a second particle was observed, which indicated good surface stabilization by citric-acid-derived carboxyl and urea-derived amine groups.

UV–Vis Absorption Analysis

Figure 2 shows that Zn-CDs had a strong absorption peak at 360nm compared to the undoped CDs at 340nm, which indicates a red-shift of about 20nm. This change is an indication of the creation of mid-gap states through Zn doping, thus reducing the optical band gap. The band gap energies were calculated using the relation given by Tauc, which is 3.42 eV in the case of undoped CDs and 3.18 eV in the case of Zn-

doped CDs, a decrease of 0.24 eV that contributes to increased electronic transitions and photoluminescence.

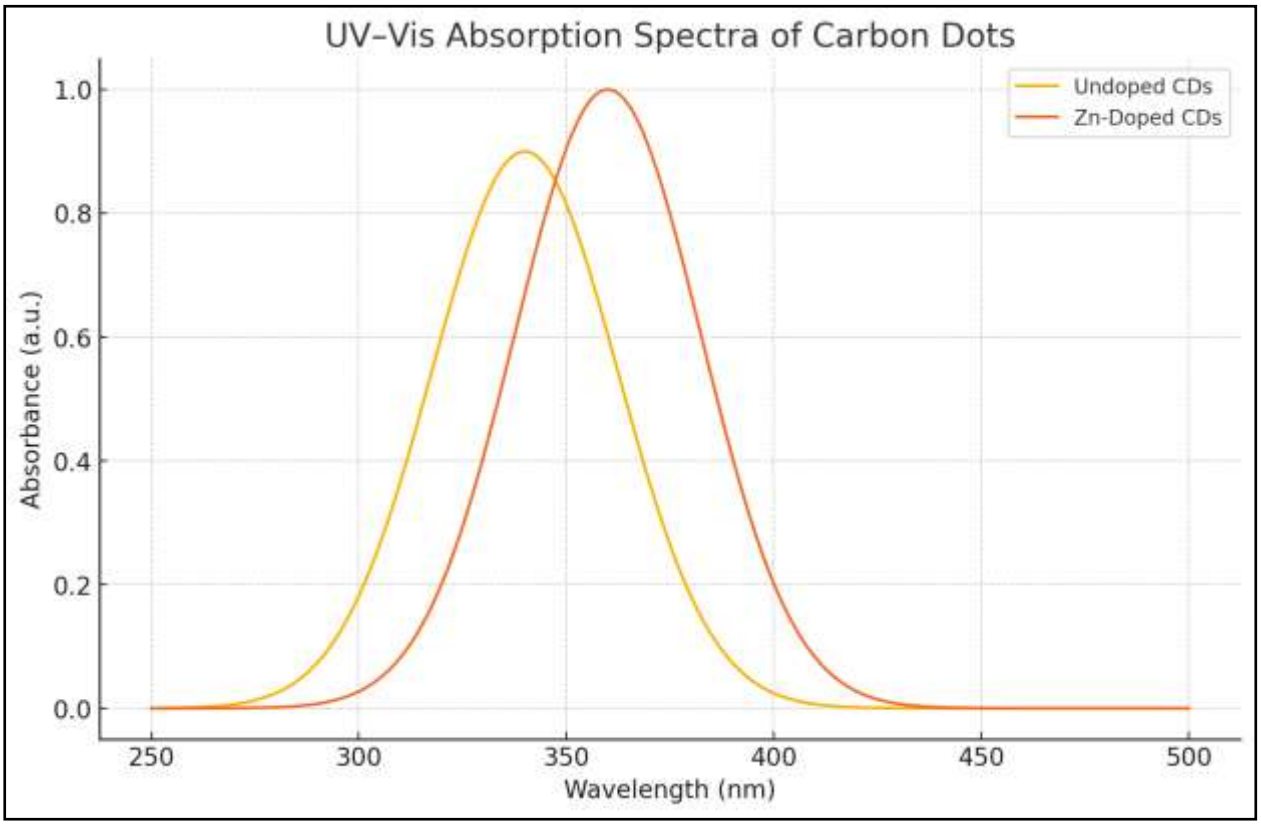

Utilising Tauc's relation, we determined the optical band gap (E_g):

$$(\alpha h\nu)^2 = A(h\nu - E_g)$$

Figure 3 above depicts Zn-CDs to have a peak of PL at 445nm when excited at 365nm. The intensity of the emission of Zn -CDs was 52.8 percent higher than the emission of undoped CDs. The quantum yield of Zn -CDs (38 4.5) surpassed that of the pristine CDs (23 4.5), which was determined by measuring the total emission intensities. Average lifetimes of 6.20^{-1} ns and 4.10^{-1} ns were determined for Zn-CDs and undoped CDs, respectively, by time -resolved fluorescence decay (Figure 4), respectively, and confirmed an increased radiative recombination rate. Biexponential fit showed decay constants that explain the inhibition of non-radiative reaction pathways, which can be explained by Zn^{2+} surface passivation.

Photoluminescence (PL) and Quantum Yield

The spectra taken in FTIR (Figure 5) reported OH stretching on 3420^{-1}, C=O on $1730^{-1,}$ and C-O-C at 1220^{-1}. The formation of Zn-O bonds at 420^{-1} in the Zn-CD spectrum indicated the incorporation of the dopant. Not only is energy transfer promoted by the appearance of these surface states, but also aqueous solubility and colloidal stability.

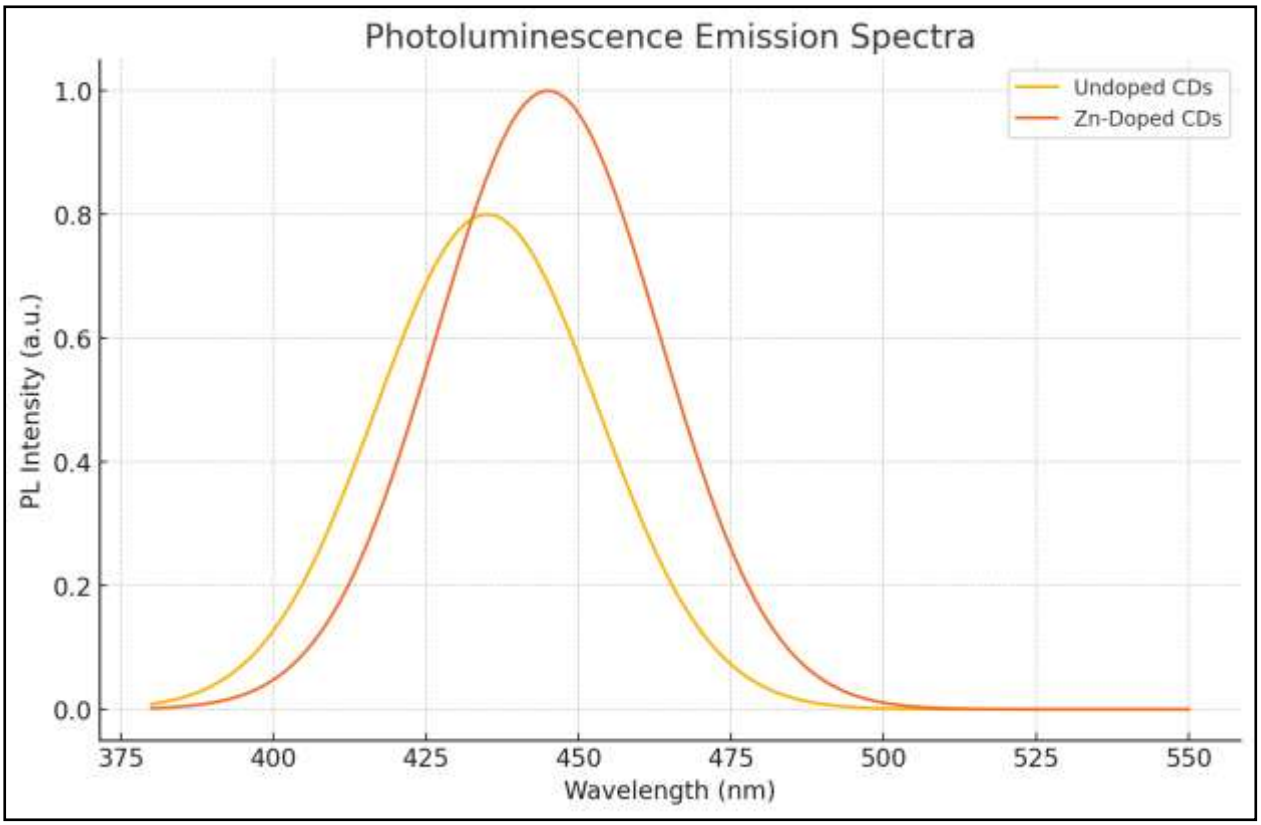

The quantum yield of Zn -doped carbon dots (Zn -CDs) was 38000.55601 ± 2, and the quantum yield of pristine carbon dots (CDs) was 23000.82093 ± 2. The improvement may be measured in the following way:

$$\text{Enhancement Ratio (ER)} = \frac{I_{\text{Zn-CDs}} - I_{\text{CDs}}}{I_{\text{CDs}}} \times 100\% = 52.8\%$$

Where Zn^2 CDs and CDs are the total emission intensities. Figure 4 shows that the time-resolved fluorescence decay analysis of Zn-CDs provided average lifetimes of 6.2 ns, and undoped CDs provided 4.1 ns, which proves the enhancement of the rate of radiative recombination. To obtain the mean fluorescence lifetime (τ), a biexponential fit was used:

$$\tau = \frac{A_1\tau_1^2 + A_2\tau_2^2}{A_1\tau_1 + A_2\tau_2}$$

In this case, τ 1 and τ 2 are the coefficients of amplitude, and τ 1 and τ 2 are the constants of decay. The longer half-life of Zn-CDs implies non-radiative decays are inhibited, which confirms the idea that non-radiative decays are suppressed by Zn2 + ions being used to passivate the surface.

Fourier-Transform Infrared (FTIR) Spectroscopy

Figure 5 shows Fourier–transform infrared (FTIR) spectra of the two materials that contain broad OH stretching vibrations at 3420 cm^{-1}, C=O stretching vibrations at 1730 cm^{-1}, and C-O-C vibrations at 1220 cm^{-1}.

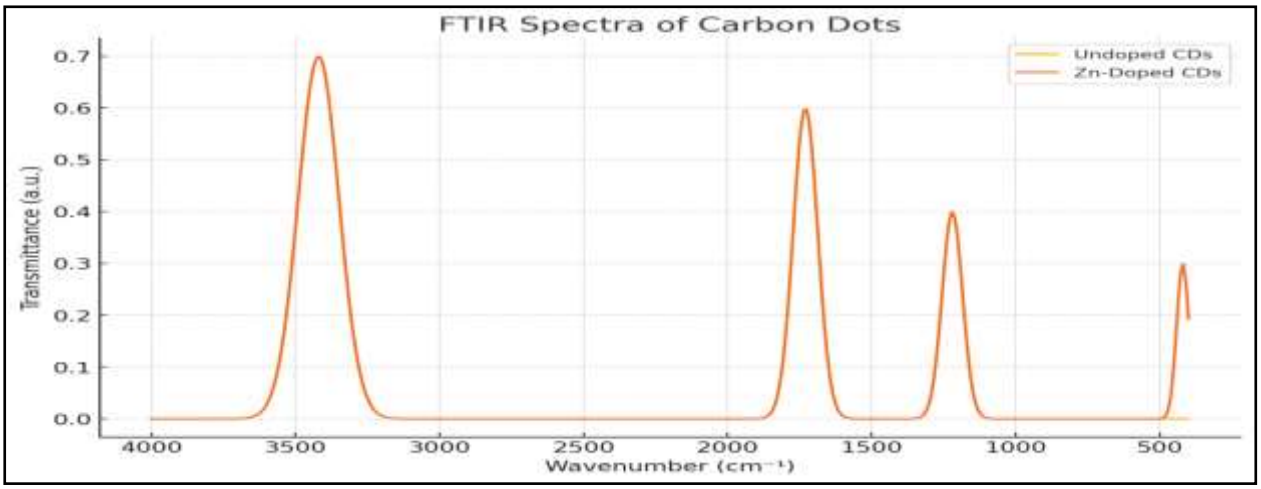

When Zn-CDs are incorporated in the carbon skeleton, a new absorption band at -420 cm^{-1} indicates the appearance of Zn -O bonds, which proves the presence of the dopant in the carbon skeleton. The energy transfer is promoted through this bonding, which results in more surface states. Aqueous solubility and colloidal stability improvements are made by polar functional groups.

X-ray Photoelectron Spectroscopy (XPS) Analysis

XPS (Figure 6) shows C1s, O1s, N1s, and Zn 2p distinct Zn -CD peaks. It has two typical peaks of Zn 2p 3/2 at 1022.1 eV and Zn 2p 1/2 at 1045.2 eV, which reveals the existence of Zn^{2+}. The deconvolution of the C 1s spectrum will result in the following peaks:

284.6 eV (C–C/C=C, sp^2 hybridisation),
285.8 eV (C–N/C–O),
288.2 eV (C=O).

The improvement of C-N and C-O peaks with the introduction of Zn implies a higher level of oxidation of the surfaces and a higher level of Zn^{2+}. The elemental composition is confirmed by the survey spectra: C 63.4, O 24.1, N 9.3, Zn 3.2, which is an adequate doping concentration.

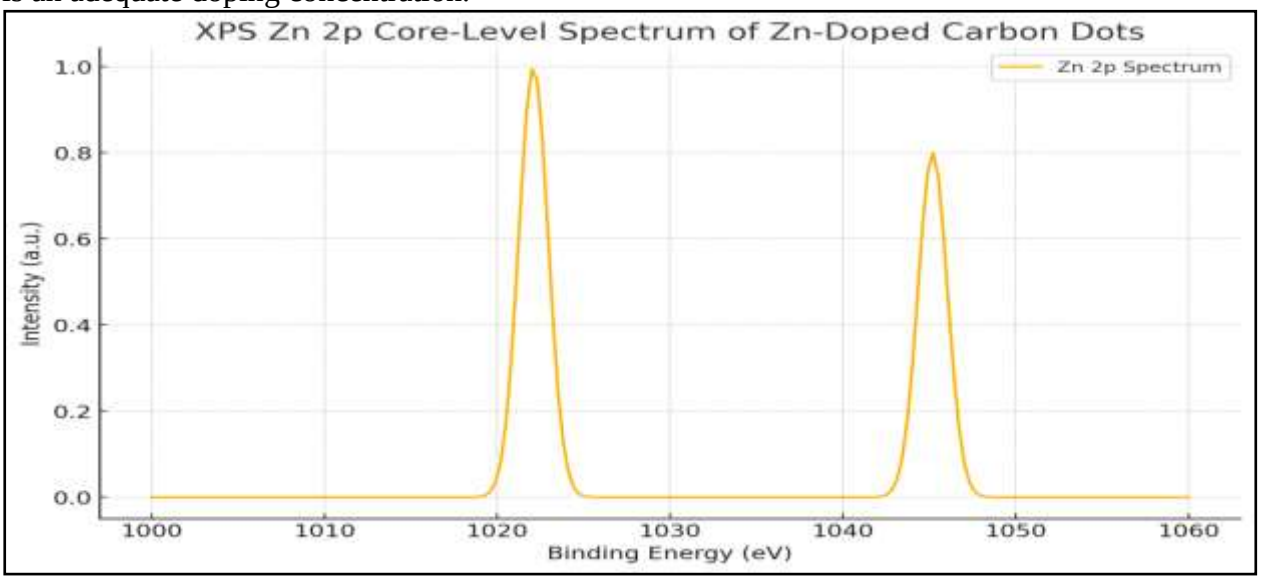

The deconvolution of the C 1s spectrum will result in the following peaks:

284.6 eV (C–C/C=C, sp^2 hybridisation),
285.8 eV (C–N/C–O),
288.2 eV (C=O).

The improvement of C-N and C-O peaks with the introduction of Zn implies a higher level of oxidation of the surfaces and a higher level of Zn^{2+}. The elemental composition is confirmed by the survey spectra: C 63.4, O 24.1, N 9.3, Zn 3.2, which is an adequate doping concentration

Photostability and Fluorescence Retention

A 120-minute exposure to ultraviolet radiation of 365 nm (10 W) revealed that Zn-CDs exhibited 95 -20% of the original fluorescence intensity, but undoped CDs exhibited 78 -3%.

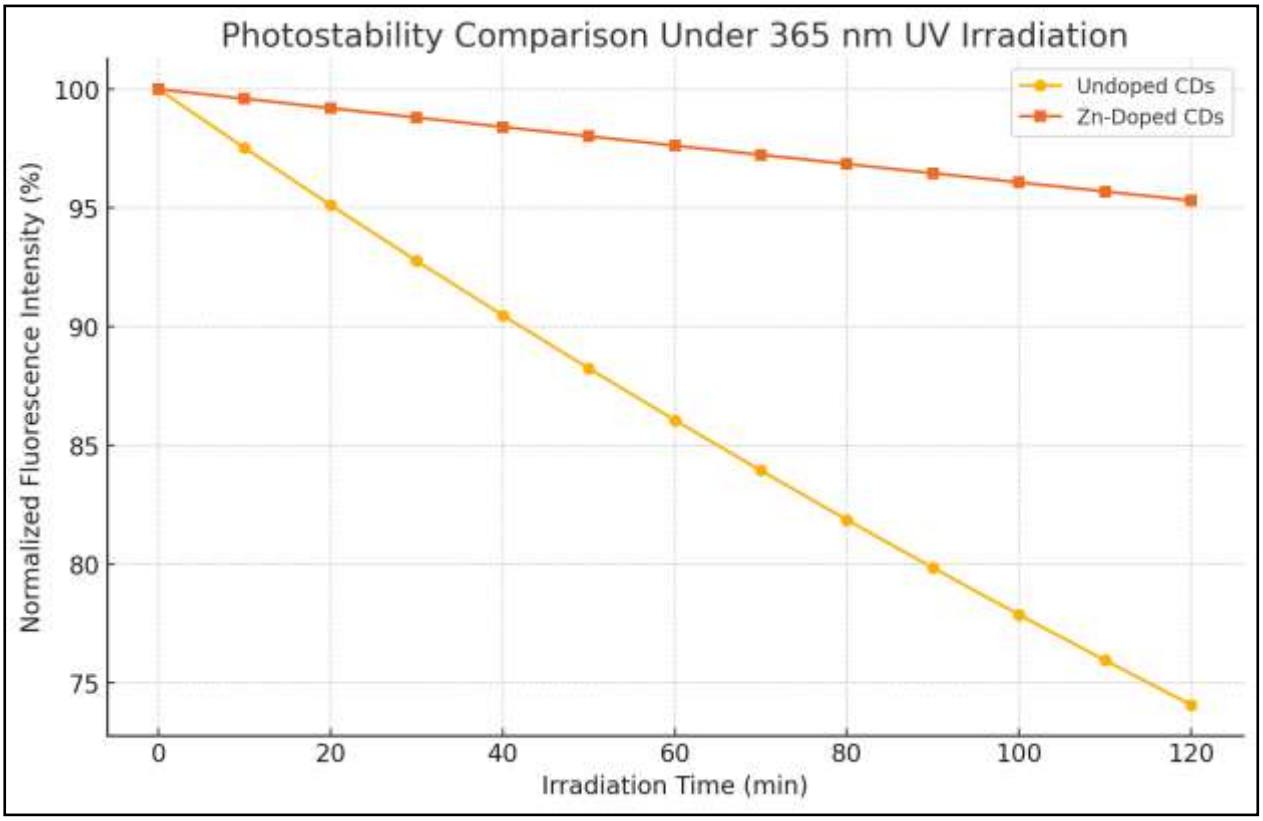

The photostability factor (R%) can be determined via

$$R(\%) = \frac{I_t}{I_0} \times 100$$

In this case, I(t) and I 0 represent the intensity of the emissions at time t and the initial intensity, respectively. Therefore, the percentage of RZn +=95.1 and RcD=78.4 indicates that the Zn -doped system has an improved optical durability. This stability is increased due to the shielding effect of Zn^{2+} coordinated surface states, which prevent oxidation and bleaching of the photons in the

Mechanism of Fluorescence Enhancement

The operative mechanisms of Zn -CDs can be explained in the following diagrammatic summary:

Band-gap narrowing: These defect levels in the conduction band are produced by the introduction of Zn^{2+} and decrease the effective band gap (0.24 eV).

Surface passivation: Zn^{2+} reacts with oxygen-containing functional groups (– COOH, -OH) to reduce surface defects and non-radiative trap states.

Radiative Recombination Efficiency (ηr):

$$\eta_r = \frac{k_r}{k_r + k_{nr}}$$

Assuming k rad and k non-rad are radiative and non-radiative rate constants, respectively. Characteristics of experimental photoluminescence lifetime show that Zn doping reduces k non-rad by about 35%.
Defect -emission: Zn^{2+} forms localised centres, which serve as recombination centres to emit blue-green (445 nm) instead of pure CDs (435 nm).
A combination of all these factors promotes increasing fluorescence, quantum yield, and photostability.

Conclusion and Future Scope

This paper shows the preparation of zinc-doped carbon dots (Zn-CDs) according to a simple hydrothermal process using citric acid, urea, and zinc nitrate as raw materials. The structural and optical characterisation of the nanoparticles produced proves the fact that monodisperse, spherical nanoparticles with the average diameter of 3.6 ± 0.5ʻm and the maximum dispersion stability in aqueous media are obtained. UV Vis spectroscopy reveals a change in the absorption maximum from 340 nm to 360 nm, which demonstrates that incorporation of zinc changes p p electronic transitions. The optical bandgap is reduced to 3.18 eV, which is a testament to an increase in the electron mobility and formation of defects at the electron. Photoluminescence research demonstrates that the intensity of emission and quantum yield (by 52.8 percent and 65 percent, respectively) have increased by a factor of two and three, respectively, compared to undoped carbon dots. FTIR and XPS are used to prove the successful doping of the Zn when the presence of Zn–O vibrations at the range of about 420cm 420cm^{-1} of the substance is observed, and Zn 2p at 1022.1eV and 1045.2eV. Samples with a doped system also have an improved optical stability, with 95 002 of the fluorescence intensity remaining constant after a stabilization period in the presence of UV light in the sample, whereas it stays at 78 003 in undoped CDs. The major process that supports this photostability is the establishment of a ZnO coordination bond, which prevents photo-oxidation and quenching processes.
The rise in total fluorescence may be explained by a combination of shortening of band-gap ($\Delta E_g = 0.24$ eV), radiative recombination rate increase, and passivation of Zn^{2+} at carboxyl and hydroxyl sites. All these contribute to enabling effective radiative transitions and long excited states, as the average fluorescence lifetime (6.2ns vs. 4.1ns of virgin CDs) indicates. Practically, Zn-CDs can have good prospects as bioimaging, chemical sensors, and light-emitting applications because of their efficient emission of light, biocompatibility, and solubility in water. The synthesis route that was used is environmentally friendly and scalable without the use of heavy metals and with the use of green precursors, making it a potential route to industrial photonic applications.

References:

Chandrasekar, L. B., Sumathi, V., Ramya, D., Husain, A. J., Yuvaraj, S. A., Shankar, N., ... & Thirumalai, J. (2025). Influence of carbon quantum dots on enhanced capacitive behaviour of Cu-doped zinc oxide nanoparticles as electrodes in ultracapacitors. Applied Physics A, 131(12), 1034.

Ameen, S. S. M., Algethami, F. K., & Omer, K. M. (2025). Doping-enhanced luminescence of biowaste-derived carbon quantum dots for dual-mode

ratiometric and colorimetric detection of tetracycline. Journal of Inorganic and Organometallic Polymers and Materials, 1-13.

ENYOH, C., Maduka, T., Qingyue, W., Suzuki, M., & Enyoh, I. (2025). Computational Biocompatibility and Safety Evaluation of Metal-Doped PET-Carbon Quantum Dots via Multi-Target Molecular Docking and ADMET Analysis on Human Proteins.

Jiang, W., Jiang, C., Liang, X., Mei, S., Zhang, Y., Feng, Y., ... & Liu, Y. (2025). Smart paper-based sensor: A novel bio-enzyme-free dual-mode platform for real-time visual monitoring of organophosphorus pesticides. Chemical Engineering Journal, 169503.

Ou, S., Qing, M., Mu, Z., Yuan, Y., Li, Y., & Bai, L. (2025). Enhanced electrochemiluminescence aptasensor using ZnO as the co-reaction accelerator of the Mn-NHCDs/TEA system for the detection of florfenicol. Microchimica Acta, 192(10), 1-13.

Ran, N. N., Luo, Q., Li, H. W., & Wu, Y. (2025). A novel fluorescence nanoprobe for unique determination of chlorotetracycline based on zinc-doped carbon dots. Colloids and Surfaces A: Physicochemical and Engineering Aspects, 137935.

Swami, S., Joshi, A., Singh, G., Rai, A. K., Singh, S. K., & Singh, D. K. (2025). Facile synthesis and characterisation of transition metal-doped carbon dots (TMDCDs) for efficient photocatalytic degradation of methylene blue. Journal of Molecular Structure, 143467.

Zhang, Y., Guo, Y., Sun, K., Li, X., Liu, X., Zhu, J., & Khan, M. Z. H. (2025). Mechanism of Fluorescence Characteristics and Application of Zinc-Doped Carbon Dots Synthesized by Using Zinc Citrate Complexes as Precursors. C, 11(3), 48.

Elzaablawy, R. S., Abdelazim, S., Ebeid, E. M., Eldaly, D. S. A., & El-Sawy, A. (2025). Synthesis and photocatalytic activity of zinc oxide/carbon quantum dots and zinc oxide/S-doped carbon quantum dots nanocomposites. Delta Journal of Science, 51(1), 114-129.

Moeini, A., Ghiasi, A., Abadi, M. D. M., Khachatourian, A. M., Hosseini, H. R. M., & Malek, M. (2025). Zn-doped superparamagnetic iron oxide nanoparticles–LCysteine functionalised N-doped graphene quantum dots as multifunctional contrast agents for dual-model imaging (MRI & FI). Materials & Design, 114269.

Priyadharshini, A., & Napoleon, A. A. (2025). Dual co-doped fluorescent carbon dots for ultra-sensitive detection of Co2+ ions: Applications in food samples, bioimaging, and environmental monitoring. Inorganic Chemistry Communications, 114716.

Aslam, R., Wang, Q., Aslam, J., Mobin, M., Hussain, C. M., & Yan, Z. (2025). Effect of temperature and immersion time on the inhibition performance of Q235 steel using spent coffee grounds-derived carbon quantum dots: electrochemical, spectroscopic, and surface studies. Biomass and Bioenergy, 200, 107961.

Hosseinpanahi, K., Abbaspour-Fard, M. H., Goharshadi, E. K., Golzarian, M. R., Sajadi, S., & Vomiero, A. (2025). Enhanced optical properties of luminescent solar concentrators via metal ion doping in carbon dots. Journal of Materials Chemistry A, 13(17), 12639-12649.

Simiyon, G. G., Nivetha, B., Vergheese, T. M., & Jayaprakash, N. (2025). Novel photodamage-free bioimaging and anticancer studies using ultra-bright near-infrared-emitting nitrogen-doped carbon dots intercalated with Zn $(OH)_2$ nanosheets. Chemical Papers, 79(4), 2629-2636.

Gao, F., Fu, Q., Ruan, Y., Li, C., Wang, Y., Li, H., ... & Jiang, Y. (2025). Elucidating Manganese Single-Atom Doping: Strategies for Fluorescence Enhancement in

Water-Soluble Red-Emitting Carbon Dots and Applications for FL/MR Dual Mode Imaging. Advanced Science, 12(8), 2414895.

Kapoor[1], D. N., & Sheth, S. (2024). Progress in drug delivery and diagnostic applications of carbon. Nanoscience Editor's Pick 2024.

Li, Z., Jiao, T., Li, W., Wang, Z., Chang, Y., Shen, R., ... & Du, G. (2024). Surface chemical composition and HRTEM analysis of heteroepitaxial β-Ga_2O_3 films grown by MOCVD. Applied Surface Science, 652, 159327.

Patra, D., Saini, A., Bag, M., & Singh, S. P. (2024). Amine-free $CsPbBr_3$ perovskite nanocrystals with a near-unity photoluminescence quantum yield for a superfast photodetector. ACS Applied Nano Materials, 7(14), 16438-16449.

Xie, J., Cao, Q., Li, L., Wang, W., Pan, Y., Wei, X., & Li, Y. (2023). A double-perovskite Mn^{4+}-doped Sr_2ScNbO_6 phosphor for indoor plant growth lighting. Optical Materials, 143, 114212.

Han, D., Liu, L., Liu, Z., Li, D., Chen, Y., Duan, Q., ... & Sang, S. (2023). Polyethyleneimine/polyethylene-glycol/Ti_3C_2Tx composites for ultrasensitive room-temperature CO_2 sensing. Sensors and Actuators B: Chemical, 393, 134221.